Application and Validation of Intelligent Inspection Robots in Aluminium Electrolysis

Junfeng Wu
Equipment Operation Superintendent
Guangxi Hualei New Materials, Pingguo, China
Corresponding author: jf_wu315@chinalco.com.cn
https://doi.org/10.71659/icsoba2025-al046

Abstract

This paper proposes an intelligent inspection robot system based on artificial intelligence (AI) technology, specifically designed for the potline basement in an aluminium smelter. The system integrates core AI technologies such as deep learning, laser simultaneous localization and mapping (SLAM) navigation, multi-sensor data fusion, and dynamic obstacle avoidance, enabling autonomous inspection under extreme conditions of high temperature, strong magnetic fields, and heavy dust. It aims to partially replace traditional manual inspections, thereby reducing labour costs while improving inspection efficiency and data accuracy. To adapt to the aforementioned extreme operating conditions in aluminium production, the system incorporates laser SLAM navigation, multi-sensor data fusion, and anti-interference communication technologies, achieving functions such as autonomous navigation, dynamic obstacle avoidance, real-time monitoring, and abnormality alarming. Moreover, by using the AI-driven multi-sensor data fusion technology, the system achieves higher reliability and adaptability, along with strong scalability, making it applicable in other industrial scenarios, such as substation inspections, and versatile across smelter-wide substation applications. All these can provide technical support and practical references for the intelligent transformation of the metallurgical industry.

Keywords: Intelligent inspection, Artificial intelligence, Laser SLAM, Aluminium electrolysis environment.

1. Introduction

1.1 Research Background and Industry Needs

As a highly energy-consuming and hazardous industrial process, aluminium production presents extreme complexity in the cell bottom. The working area is continuously exposed to multiple harsh conditions, including high temperatures (ranging from 10–15 °C in winter to 35–40 °C in summer), strong magnetic fields (up to 400 gauss), and heavy dust pollution. Traditional manual inspection methods face significant challenges: on the one hand, operators need to frequently enter the basement to perform critical temperature measurements on collector bars and cell bottom (with 120–210 measurement points per cell), exposing them to direct safety hazards such as falling carbon residues and electrical hazards. On the other hand, manual inspection suffers from low efficiency (approximately 15 minutes per cell), high subjective bias in data recording, and an inability to achieve continuous 24-hour monitoring, which results in delayed warnings of abnormal temperature rise. According to the measurements from Guangxi Hualei Aluminium Smelter, manual inspections cover only about 50 % of the cells per hour, which severely impacts production safety and process optimization.

In addition, Chinese national policies have set clear requirements for more intelligent industries. The *Robotics+ Application Action Implementation Plan* emphasizes that by 2025, the number of robots in the manufacturing sector shall be doubled, while the *14th Five-Year Plan for the Development of the Robotics Industry* further highlights the need to achieve breakthroughs in

innovative applications of robots under complex scenarios. These policy orientations are highly consistent with the aluminium industry's urgent demand for the transformation of "reduced manpower and unmanned operation", which provides strategic support for the implementation of intelligent inspection technologies [1].

1.2 Research Objectives and Significance

This study aims to develop an intelligent inspection robot system based on multi-modal perception to address the core challenges associated with basement monitoring in aluminium cells. The system design focuses on three primary objectives:

- First, by leveraging laser SLAM navigation, a four-wheel-drive obstacle-crossing chassis (with a minimum obstacle crossing height of 50 mm), and an IP55-rated structure, the system achieves autonomous mobility and precise positioning in high-interference environments；
- Second, through the integration of different sensing technologies including infrared thermal imaging (temperature measurement accuracy of ±2 °C), ultrasonic obstacle avoidance, and visible-light video, the system establishes a framework for real-time temperature rise monitoring and early anomaly warning；
- Third, supported by an anti-strong-magnetic wireless network and a layered control architecture, the system ensures continuous data return and enables remote collaborative management.

The value of this solution is reflected in two dimensions: safety and efficiency. In terms of safety, it can reduce human intervention in hazardous areas by 80 %, while sound-light alarms and emergency stop mechanisms reduce the response time to abnormal events to within 10 seconds. In terms of efficiency, the robot can operate continuously for 8 hours and cover 38 cells each day. Combined with temperature trend analysis, it provides a solid data foundation for preventive maintenance. Furthermore, the study verifies the universality of multimodal perception technology in hazardous industrial scenarios to offer a technological paradigm for intelligent upgrades in metallurgy, chemical engineering, and other industries, thereby meeting the requirements for industrialized implementation of the national "Robotics+" strategy.

Figure 1. Inspection robot in charging standby mode.

2. System Architecture and Hardware Design

2.1 Layered System Architecture

2.1.1 Layered Design

The intelligent cell bottom inspection system for aluminium cells uses a layered architecture design, consisting of the terminal layer, network layer, and application layer, thereby forming a closed-loop process for data acquisition, transmission, and management [2] (Table 1). The terminal layer is composed of mobile inspection robots and fixed-point temperature sensors. The network layer ensures reliable data transmission through magnetic field-immune wireless communication technology. The application layer integrates an intelligent management platform that supports data analysis and decision-making.

Table 1. Layered system architecture.

Layer	Components & Functions	Technical Parameters & Design Highlights
Terminal Layer	Inspection Robot (ARIS-MS100), Fixed-Point Temperature Measurement Devices	Robot dimensions up to 772 × 400 × 722 mm, IP55 rating, high magnetic field immunity (400 gauss), four-wheel drive, obstacle crossing height from 50 mm; fixed-point devices for blind-spot temperature monitoring.
Network Layer	Magnetic field-immune Wireless Access Points (AP) (56 units), Access Switches (8 ports), Aggregation Switches (workshop-level), Core Switch (centralized control centre)	APs with magnetic field immunity; optical fibre transmission bandwidth of at least 1 Gbps; wireless coverage radius of at least 500 m; network latency up to 50 ms; resumable data transfer.
Application Layer	Backend Management System (task scheduling, data analysis), AI Algorithm Module (temperature trend prediction), Interactive Terminals (PC/mobile)	Concurrent multitasking; configurable temperature alarm thresholds (±2 ℃ accuracy); minimum data retention of 3 years; visualization interface with a response time of up to 1 s.

(1) Terminal Layer Analysis

The terminal layer consists of the ARIS-MS100 inspection robot and fixed-point temperature measurement devices. The robot is equipped with a four-wheel-drive chassis with a minimum obstacle-crossing height of 50 mm, facilitating operation in environments with aluminium slag accumulation in the cell basement. Its multimodal perception module integrates a LiDAR, an infrared thermal imager (with a resolution of 640 × 512 pixels and a temperature range from 0 to 550 ℃), and ultrasonic obstacle avoidance sensors, enabling the detection of cell collector bars and cell bottom temperature as well as the activation of abnormal alarms triggered when the collector bar temperature exceeds 300 ℃. Fixed-point sensors are deployed in the robot's blind spots to supplement temperature data wirelessly and establish a comprehensive monitoring network.

(2) Network Layer Analysis

The network layer uses magnetic field-immune wireless APs (Access Points) that each provides a coverage radius of 500 m to establish redundant communication links. With 56 APs deployed in the cell bottom the communication stability under a strong magnetic field of 400 G (with a

packet loss rate below 0.1 %) is ensured [3]. The network topology is divided into an access layer, an aggregation layer, and a core layer (Figure 2): access switches connect APs in each work area with the robots; aggregation switches consolidate workshop data to the network video recorders (NVRs) and sub-control servers; the core switch connects the centralized control centre via optical fibre, enabling cross-workshop data sharing. The communication protocol supports both TCP and UDP. In the event of a network outage, robots perform offline inspections, store task data locally, and automatically resume transmission once the network is restored.

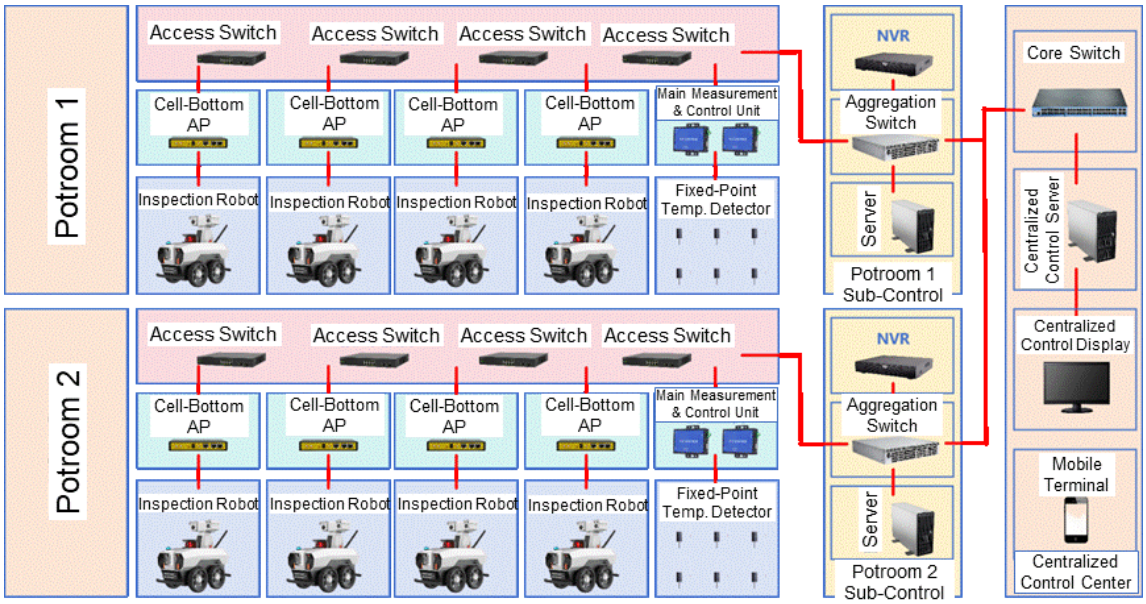

Figure 2. Schematic diagram of the network topology.

(3) Application Layer Analysis

The application layer has an intelligent management platform with functional modules including task scheduling, real-time monitoring, and data analysis. The platform uses a B/S architecture and supports multi-terminal access. The task management module provides both comprehensive inspection and customized inspection modes to support dynamic path planning. The data analysis module integrates horizontal comparison of individual cell temperatures and vertical trend prediction algorithms [4], facilitating the activation of a three-level alarm system (general/moderate/severe) when abnormal data is detected. Compatible with the GB/T 28181 protocol, the data interface integrates with the Manufacturing Execution System (MES) system of the smelter and sends the equipment status to the production management system in real time.

2.1.2 Power Supply Topology Design

The power supply topology uses a three-level redundant design (Figure 3), consisting of power input, power distribution units, and the charging system, ensuring power stability in extreme industrial environments. The variable frequency drive (VFD) serves as the core power regulation unit, receiving 380 Vac three-phase input from the smelter grid. Through harmonic suppression and voltage fluctuation compensation (±5 % accuracy), it delivers a standardized 220 Vac output to the distribution box. The distribution box is equipped with circuit breaker protection and surge suppression modules, featuring two separate output circuits:

- Robot charging circuit: connects the charging pile via magnetic shielded cables, with an input voltage range of 180–260 Vac/45–65 Hz, ensuring compatibility with voltage fluctuations in potrooms. Integrating an intelligent identification module, the charging pile supports CC–CV (Constant Current-Constant Voltage) charging for 56.4 V lithium

batteries (constant current at 20 A and switches to constant voltage until cut-off at 1 A), with a single charging cycle up to 2 hours.

- Equipment power supply circuit: powers the servers, wireless APs, and switches through independent conduits, and deploys a UPS backup power system to ensure continuous operation of network-layer equipment for at least 30 minutes in the event of a power outage.

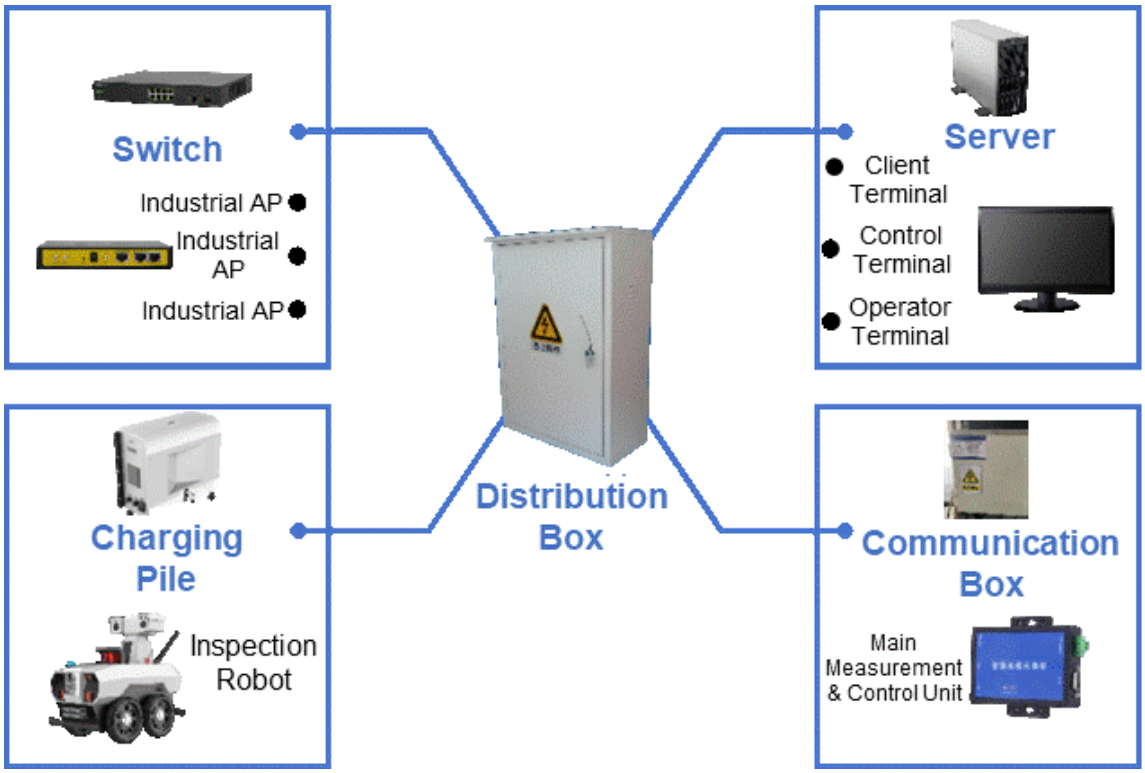

Figure 3. Schematic diagram of the power supply topology.

A purging and dedusting system is equipped in the charging room. After the robot completes the charging connection, a high-pressure airflow is triggered to clean the surfaces of the gimbal and LiDAR, thereby removing dust and preventing degradation of optical component performance. The power supply network and communication optical cables are physically isolated and armoured shielded, which can provide an electromagnetic interference resistance of at least 60 dB to ensure zero-fault operation in a 400-gauss strong magnetic environment.

2.2 Robot Hardware Configuration

2.2.1 Magnetic Field-immune Structural Design Parameters

The IP55-rated robot effectively prevents dust ingress and resists low-pressure water jets; the electromagnetic shielding design integrates composite metal laminates with double-shielded cables to mitigate the impact of strong magnetic fields on internal circuits. The overall structure is compact with a width of up to 400 mm, making it suitable for the narrow channels at the bottom of the cells. A magnetic isolation communication module ensures stable transmission of wireless signals under a 400-gauss magnetic field with a packet loss rate of less than 0.1 %.

Table 2. Anti-magnetic structural design parameters.

Design Element	Technical Parameters and Implementation Method
Protection rating	IP55 (dust-proof and protected against low-pressure water jets)
Electromagnetic shielding	Composite metal laminates (relative magnetic permeability: at least 1000 – e.g. soft iron); double-braided shielded internal cables
Strong magnetic adaptability	Continuous operation in a 400 G magnetic field; communication module equipped with magnetic isolation technology (isolation voltage: at least 2500 V)
Structural dimensions	Up to 772 mm (L) × 400 mm (W) × 722 mm (H)

2.2.2 Four-Wheel Drive Chassis and Obstacle-Crossing Parameters

The robot chassis uses an independent four-wheel drive system with a single-wheel torque of at least 35 N·m, adapting to the aluminium slag accumulation and uneven floor conditions at the cell bottom. With a minimum obstacle-crossing height of 50 mm and a climbing angle of 15°, it navigates smoothly through environments containing slag deposits and temporary obstacles. The four-wheel drive power distribution algorithm dynamically adjusts wheel speed differentials to reduce the probability of slippage and ensure stability of the inspection path.

Table 3. Four-wheel drive chassis parameters.

Performance Indicator	Technical Parameters
Drive type	Four-wheel independent drive (single-wheel torque ≥ 35 N·m)
Minimum obstacle-crossing height	50 mm
Maximum climbing angle	At least 15°
Width compatibility, passability	Minimum passage width of 500 mm; maximum trench-crossing width of 50 mm

2.2.3 Multimodal Sensors

The LiDAR (16-line, 20 Hz) integrated with an inertial measurement unit (IMU) enables high-precision simultaneous localization and mapping (SLAM) positioning, with a localization error below 20 mm. The infrared thermal imager meets the temperature measurement requirements of cell collector bars and cell bottoms, and will activate a three-level alarm system when a temperature exceed 300 °C. Ultrasonic sensors are combined with bumper strips to create a dual obstacle-avoidance system: the ultrasonic sensors detect obstacles within 1.5 m in advance, prompting the robot to reduce speed; the bumper strips trigger an immediate emergency stop upon contact. The gimbal integrates dual-mode imaging of visible light (2560 × 1440 resolution) and infrared, it supports 360° panoramic monitoring without blind spots.

Table 4. Sensor specifications.

Sensor Type	Technical Parameters and Functions
LiDAR	16-line laser SLAM, scanning frequency: 20 Hz, ranging accuracy: ±30 mm
Infrared Thermal Imager	Resolution: 640 × 512, temperature range: from 0 °C to 550 °C, accuracy: ±2 °C
Ultrasonic Sensor	Detection distance: 0.1–1.5 m, bidirectional conical field of view
Bumper Strip	Trigger pressure: up to 5 N, response time: up to 0.1 s

2.2.4 Software Platform Functions

The task management module is responsible for the planning and execution of inspection tasks. It supports multiple modes including comprehensive inspection, customized inspection, manual inspection, and nighttime inspection [5]. In the comprehensive inspection mode, the robot follows a preset path to perform full coverage detection of all temperature measurement points at the cell bottom, with approximately 210 measurement points per cell. The customized inspection mode allows users to define inspection items based on specific requirements. When abnormal data are detected, the system automatically initiates targeted inspections. The inspection path is globally planned using laser SLAM technology. Combined with dynamic path optimization algorithms, it ensures efficient obstacle avoidance and precise localization in complex environments. Task dispatch logic supports both remote control and automated scheduling, enabling users to start or terminate inspection tasks with a single click through the backend system.

Built on a B/S architecture, the real-time monitoring module integrates both visible light and infrared thermal imaging video streams, and supports remote access across multiple terminals. Users can monitor the cell bottom in real time via PC or mobile devices. Voice alarms will be triggered in case of abnormalities. Leveraging the temperature trend prediction algorithm embedded in the data analysis module, it supports horizontal comparison of single-cell temperatures and vertical analysis of historical data. Alarm thresholds can be flexibly configured according to process requirements: an immediate alarm is triggered when the square steel bar temperature exceeds 300 °C; an early warning is automatically issued if the cell-bottom temperature rises by more than 20 °C. With the data visualization function, temperature variation curves, thermal imaging maps, and statistical reports of abnormality can be created to assist Operation & Maintenance (O&M) personnel in rapid decision-making. The module also supports breakpoint-resume data transmission, stores task data locally during network interruptions and automatically uploads it to the backend upon recovery.

Figure 4. Monitoring system operation interface.

3. Key Technology Implementation

3.1 Autonomous Navigation and Dynamic Obstacle Avoidance

The laser SLAM (Simultaneous Localization and Mapping) technology is based on a 16-line high-precision LiDAR (angular resolution: 0.33°, detection radius: 30 m) to construct a two-dimensional grid map of the cell bottom. Data from the IMU (three-axis accelerometer: ±16 g, gyroscope: ±2000 °/s) and wheel odometry (encoder accuracy: 0.1 mm) are fused through Extended Kalman Filtering (EKF) with a positioning error of up to ±20 mm. The SLAM algorithm uses the Gmapping framework based on Rao-Blackwellized Particle Filtering to update environmental point clouds in real time (update frequency: 10 Hz) and accommodate dynamic changes such as material spillage at the cell bottom and equipment displacement. Global path planning is implemented using an improved A* algorithm with Manhattan distance as the heuristic function to minimize the inspection path across 38 cells (total travel distance reduced by 18.7 %). For local obstacle avoidance, the Dynamic Window Approach (DWA) is employed to calculate five sets of velocity vectors (linear velocity: 0–1.5 m/s, angular velocity: 0–1.2 rad/s), and the optimal solution is selected based on the maximum evaluation function (goal proximity, obstacle clearance, and velocity smoothness) with a response latency of at least 200 ms.

The dynamic obstacle avoidance strategy divides the response zones into three levels: warning zone (1.5–2.0 m), deceleration zone (1.0–1.5 m), and stop zone (below 1.0 m).

The LiDAR sensor (horizontal FOV: 270°) detects obstacles and applies a segmented velocity attenuation function:

- Warning zone: maintains a velocity of 0.8 m/s, with acoustic and visual warnings;
- Deceleration zone: velocity linearly decreases to 0.1 m/s (attenuation slope: –0.7 m/s²);
- Stop zone: drive motor torque drops to zero, and the dual-redundant braking system (electromagnetic brake and mechanical brake) halts the robot within 80 ms. An ultrasonic sensor (40 kHz, 60° detection angle) supplements the detection of low obstacles with a height of no higher than 200 mm and forms a heterogeneous sensing network together with bumpers (trigger threshold: 5 N), with an error rate of less than 0.5 %.

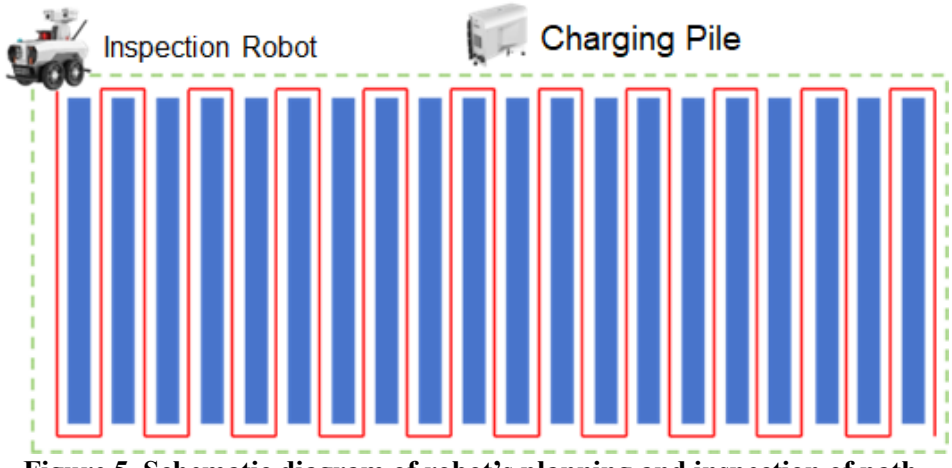

Figure 5. Schematic diagram of robot's planning and inspection of path.

3.2 Multi-Sensor Data Fusion

The infrared thermal imager (Noise Equivalent Temperature Difference below 50 mK) captures the temperature field at the cell bottom at a sampling rate of 10 Hz. The visible-light camera

(minimum illumination: 0.01 Lux) simultaneously records video streams in 4K. A spatiotemporal registration algorithm computes the spatial mapping relationship between the two based on the gimbal's pose (pitch angle: ±0.1°, yaw angle: ±0.05°) to establish a temperature–pixel correspondence model, Equation (1):

$$\begin{cases} x_{IR} = k_x \cdot x_{VIS} + b_x \\ y_{IR} = k_y \cdot y_{VIS} + b_y \end{cases} \quad (1)$$

where:
k_x, k_y Scaling factors
b_x, b_y Offsets with a registration error of up to 3 pixels.

Temperature anomaly points (more than 300 °C) are denoised using morphological filtering. The FLANN (Fast Library for Approximate Nearest Neighbours) algorithm is applied to match equipment contours in visible-light images with a localization accuracy of ±1.5 cm.

The anti-fall algorithm fuses the data from ultrasonic sensors (resolution: 1 mm), tilt sensors (measurement range: ±30°), and IMU. An ultrasonic array (two sets each at the front and rear) continuously monitors the ground clearance of the chassis. When a sudden height change of more than 50 mm is detected, or echo signals are lost for 5 consecutive frames, a three-level response system is initiated:

- Baseline response: the speed is limited to 0.2 m/s, and the gimbal returns to centre.
- Escalated response: if the tilt angle exceeds 8°, differential steering is enabled for attitude compensation.
- Emergency response: when the tilt angle exceeds 15° or the height difference exceeds 80 mm, the drive power is cut off and mechanical support legs are extended.

Kalman filtering (process noise Q = 0.01, observation noise R = 0.1) is employed to eliminate signal jitter caused by dust, with an error rate of less than 0.05 %. The braking process uses PID control ($K_p = 12.5$, $K_i = 0.8$, $K_d = 2.2$) to ensure a stopping distance of up to 50 mm.

3.3 Anti-Interference and Reliability Verification

The wireless communication system uses a dual-layer magnetic shielding structure, with a μ-metal alloy layer (or soft iron, the relative magnetic permeability being at least 5000) embedded in the AP housing, an internal circuit board with 2 oz copper cladding, and a grounding impedance of less than 0.1 Ω to effectively suppress the eddy current effects caused by a 400-gauss magnetic field. The communication protocol employs Adaptive Frequency Hopping Spread Spectrum (FHSS, 80 frequency points) to dynamically switch channels in the 2.4 GHz band (switching time: less than 50 ms) and improve the signal-to-noise ratio by 12 dB. At the data link layer, CRC-32 error detection and retransmission mechanisms (maximum 3 retries) are implemented to keep the packet loss rate below 0.1 %.

In offline inspection mode, the robot's local storage unit (eMMC 64 GB) caches inspection data partitioned by task ID. When a network interruption occurs, the task progress is marked as a "breakpoint," and an MD5 checksum (128-bit hash length) is generated in real time to ensure data integrity. After network recovery, the incremental upload module, based on RESTful API, compares the latest task ID on the server and transmits only the differential data (compression ratio: at least 70 %), with a breakpoint resume latency of less than 2 seconds.

3.4 Endurance and Charging Optimization

The charging pile integrates a dual-mode switching logic: in automatic mode, the robot uses AprilTag visual markers (15 × 15 cm, recognition distance: 1.5 m) to align with the charging plate with a positioning accuracy of ±3 mm; in manual mode, the Type-C fast charging interface (PD3.0) is enabled to support 56.4 V/20 A input. During the charging process, the robot usess a constant current–constant voltage (CC-CV) switching control strategy: in the constant current phase (20 A), the battery is rapidly charged to 95 % of its capacity; in the constant voltage phase (56.4 V), it is trickle charged to 100 %. A temperature monitoring module (Negative Temperature Coefficient thermistor of 10 kΩ at 25 °C) limits the cell temperature difference within 2 °C.

The robot is equipped with lithium iron phosphate ($LiFePO_4$) batteries (nominal capacity: 50 Ah). After 1 500 charge-discharge cycles at 0.5 C (charging rate, here the nominal capacity is charged in 2 hours with a current of 25 A), the capacity retention remains at least 80 %. The lifetime model, based on the Arrhenius equation (activation energy Ea = 35 kJ/mol), predicts a cycle life of up to 2 300 cycles at 25 °C (with capacity fading to 70 %) under well-protected conditions. With algorithm-based dynamic optimization, the robot reduces its overall energy consumption by 37 % during low-speed inspection (0.5 m/s) by disabling the gimbal motors and lowering the infrared thermal imager sampling rate from 10 Hz to 5 Hz.

4. Industrial Applications and Effectiveness Analysis

4.1 Real-world Application and Operational Performance

At Guangxi Hualei Aluminium Smelter, 300 units of 500 kA cells are distributed across 8 operation zones, with each zone containing 37–38 cells. The inspection area at the cell bottom is arranged orderly, with channel widths at least 500 mm. The project uses a layered deployment: each operation zone is equipped with one ARIS-MS100 inspection robot and 56 magnetic field-immune wireless APs to form a three-layer network architecture of “Robot–AP–Switch”. The robot charging rooms are located at the edge of the cell bottom, with an input voltage of 180–260 Vac to support automatic docking and charging, as well as breakpoint resume. The system covers critical temperature measurement points at the cell bottom and square steel bars, with each cell having up to 210 temperature points. Blind spots are supplemented by fixed sensors, achieving a temperature measurement coverage rate of at least 98 %.

Table 5. Measurements of the robot.

Indicators	Measurement
Single-cell average inspection time	15
Number of cells completed per day	38 cells/day
Average daily inspection frequency	Twice
Response time for anomalies	Up to10
Data loss rate	Below 0.5 %
Identification Accuracy of abnormal temperature rise	At least 95 %

According to the measured data (Table 5), a single robot inspects an average of 38 cells per day with 15 minutes per cell, demonstrating an efficiency 2.3 times higher than manual inspection. For each cell, the robot’s infrared thermal imager measures 120 temperature points on the collector bars within 12 minutes, with the remaining 3 minutes dedicated to the identification of the hottest points at the cell bottom and data transmission. The system uses dynamic priority scheduling algorithm to automatically mark abnormal cells, with a response time of up to 10 seconds. Compared to manual inspection, which takes 15 minutes per cell with only 50 %

coverage, the robot provides 24-hour continuous monitoring, with a data loss rate of less than 0.5 % and an abnormal temperature rise (ΔT is at least 20 °C/h) detection accuracy of at least 95 %.

4.2 Safety and Economic Benefits

4.2.1 Safety Effectiveness

In the aluminium smelter's cell-bottom environment, carbon residue falling, strong magnetic radiation, and high-temperature pose significant safety threats. In traditional manual inspection, operators access the cell bottom 2–4 times daily, each time lasting 15–30 minutes. After the deployment of the ARIS-MS100 inspection robot, the frequency of human intervention in hazardous areas is reduced by 80 %. By utilizing LiDAR and bumper strips, the robot achieves fully autonomous obstacle avoidance and eliminates the risk of exposure to falling carbon residue. Data from Guangxi Hualei Aluminium Smelter indicate that the robot replaces an average of 38 manual inspection tasks per day and reduces potential personal injury incidents by approximately 120 cases annually.

The system uses a three-level alarm system (general/moderate/severe) and integrates audible-visual alarms with backend pop-up warnings. When the infrared thermal imager detects that the collector bar temperature exceeds 300 °C, an audible-visual alarm (response time: up to 10 seconds) is triggered immediately, and abnormal data is sent back in real time to the backend via magnetic field-immune wireless APs. Compared with the average manual inspection response time of 15 minutes, the robot improves abnormal event handling efficiency by a factor of 90. The backend system automatically generates event logs and pushes them to the MES platform. O&M personnel check thermal imaging maps and temperature trend curves in real time via mobile devices to achieve closed-loop management of anomaly detection and handling.

4.2.2 Economic Benefits

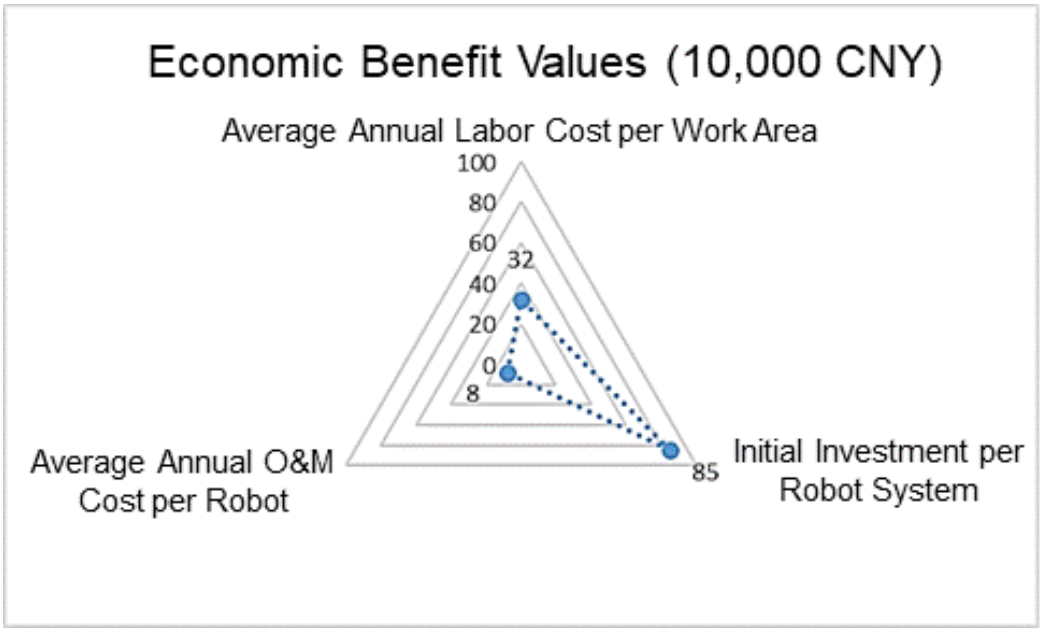

Figure 6. Radar chart of economic benefits.

As shown in Figure 6, the average annual cost of manual inspection per work area includes labour wages (2 personnels × 120 000 CNY/p.year, 13.8 kUSD/p.y approx.), protective equipment (30 000 CNY/year, 4.15 kUSD/y approx.), and accident compensation reserve (50 000 CNY/year,

6.9 kUSD/y approx.), totalling 320 000 CNY (44.3 kUSD/y approx.). The initial investment for a robotic system (about 850 000 CNY – 118 kUSD approx. – for the robot and its supporting equipment) has a ROI cycle of 2.7 years. The subsequent O&M cost (including energy consumption, maintenance, and battery replacement) is about 80 000 CNY (12.2 kUSD approx), representing a 75 % reduction compared with manual inspection. Based on the deployment of seven robots across eight work areas at Guangxi Hualei Aluminium Smelter, the total cost savings over a five-year cycle amount to 11.2 million CNY (1.55 MUSD/5 y approx.).

Through the vertical analysis of temperature trend at square steel bars ($\Delta T \geq 20$ °C/h), the system provides early warning of potential cell leakage risks up to 48 hours in advance, reducing unplanned downtime by 65 %. Continuous monitoring data from the robot supports comprehensive assessment of cell health. A single unplanned shutdown results in a production loss of approximately 500 000 CNY per hour (69 kUSD/h approx.). With robots deployed, an average of 120 hours of annual downtime is reduced, directly safeguarding production capacity valued at 60 million CNY (8.3 MUSD/y approx.). It ensures an abnormal temperature rise detection accuracy of no less than 95 %, a false alarm rate of less than 2 %, reduces unnecessary maintenance tasks and saves an average of 2.8 million CNY in maintenance costs per year (390 USD/y approx.).

5. Conclusions and Expanded Applications

5.1 Summary of Research Findings

The large-scale deployment of the intelligent inspection robot system at Guangxi Hualei Aluminium Smelter, consisting of 300 units of 500 kA cells, has validated the technical feasibility of operation in extreme industrial environments. The IP55 protection rating and a magnetic field-immune design that withstands 400 G ensure the system's stable performance under high-temperature conditions (–10 to 50 °C), dusty environments (PM10 up to 5 mg/m^3), and strong magnetic field, with an average daily coverage of 38 cells. Leveraging multimodal perception technologies, which include laser SLAM (positioning accuracy: ±20 mm), infrared thermal imaging (temperature measurement accuracy: ±2 °C), and ultrasonic obstacle avoidance (detection range: 1.5 m), the system reduces the cell bottom temperature data loss rate from 50 % (manual inspection) to 0.5 % and improves data continuity by a factor of 12.

The system's dynamic path planning and three-level obstacle avoidance mechanism enable autonomous navigation through aluminium slag accumulation zones at the cell bottom (minimum obstacle-crossing height of 50 mm) with an abnormal temperature rise (ΔT at least 20 °C/h) identification accuracy of at least 95 %. The multi-source data fusion algorithm supports horizontal single-cell temperature comparison and vertical trend prediction, and reduces the leakage risk warning time from a 2-hour delay in manual inspection to a 48-hour advance notice.

5.2 Technical Scalability

The expansion of inspection to distribution rooms requires addressing the challenge of three-dimensional navigation in narrow spaces (passage width up to 500 mm). While current laser SLAM technology can adapt to two-dimensional planar paths, it must be integrated with ToF depth sensors to achieve stereoscopic obstacle avoidance. The fault prediction capability of industry-specific small models can be optimized through transfer learning: by training an LSTM time-series model on 100 000 sets of historical temperature rise data collected at the bottom of aluminium cells, the prediction error rate can be reduced to below 3 %.

The AI-driven layered architecture supports edge computing and cloud collaboration: the front-end robot performs real-time anomaly detection (response latency up to 1 second). The backend

platform employs convolutional neural networks (CNN) to analyse infrared thermal imaging maps, and identifies local overheating caused by micron-scale carbon slag accumulation. Algorithm optimization includes lightweight model deployment (parameter size up to 1 million) and enhanced robustness against adversarial samples, reducing the false alarm rate to 1 %.

5.3 Industrial Application Value

In close alignment with Chinese national policies, the technical architecture of the intelligent inspection robot system facilitates the use of these policies as carriers of technical references, enabling the development of replicable, standardized solutions. In response to the *"Robotics+" Implementation Plan*, the system achieves a substitution rate of at least 80 % in hazardous scenarios to meet the inspection requirements for ledges. Through laser SLAM navigation and multi-modal perception technologies, it enables continuous temperature monitoring of high-temperature ladles (at least 800 °C), significantly reducing the frequency of human intervention. In line with the *14th Five-Year Plan for the Development of the Robotics Industry,* the system's multi-modal perception patents account for 35 % of the total, and its fusion algorithm, which combines infrared thermography and ultrasonic sensing, can be expanded to leakage monitoring in chemical reactors and accurately identify local overheating (ΔT at least 5 °C/min) caused by micro-scale cracks.

The standardized design should be further adapted to inspection scenarios in the radiation zones of nuclear power plants. This is demonstrated by the system's ability to increase data acquisition frequency from 0.1 Hz to 10 Hz, thereby meeting the stringent real-time monitoring requirements of nuclear facilities. Combined with a radiation-hardened reinforced structure (IP68-rated) and an anti-interference communication module (packet loss rate below 0.1 %), the system enables fully unmanned operation and maintenance in hazardous areas. The robot's four-wheel-drive chassis (torque at least 35 N·m) and modular sensor interfaces support rapid customization, reducing deployment cycle time by 60 %. As a result, the system can be deployed within one week in applications such as ladle temperature monitoring in the metallurgical industry and corrosion detection in chemical pipelines.

In the future, by actively opening data interfaces (GB/T 28181 protocol) and enhancing the transfer learning capabilities of industry-specific small-scale models, the system can provide end-to-end solutions for high-risk industrial scenarios to support the industrialized implementation of the national "Robotics+" strategy.

6. References

1. Zhongbo Duan and Xiaogang Tian, Application Practice of Intelligent Inspection Robots in Aluminium Electrolysis Rectifier Systems, *Gansu Metallurgy*, 2022, 44(01): 93-96 (in Chinese).
2. Lang Wang et al., High-Precision Data Acquisition Method for Electrical Equipment in Water Diversion Project Stations Based on Inspection Robot Technology, *Electrical Technology and Economy*, 2025, (05): 243-245 (in Chinese).
3. Yeting Yao, Autonomous Generation Method of Intelligent Inspection Points for Substation Robots under 5G Networks, *Automation and Instrumentation,* 2025, (05): 172-175+185 (in Chinese).
4. Fenghua Liu, Lihui Yuan and Wenhui Gong, Autonomous Obstacle-Crossing Control of Intelligent Inspection Robots Based on Improved PRRT Algorithm, *Computer Measurement and Control*, 1-9 [2025-06-14] (in Chinese).
5. Guidong Wang et al., Intelligent Fault Detection System for Electrolytic Copper Cathode Plates Based on Rail-Mounted Inspection Robots and YOLO-V5, *Mining and Metallurgy*, 2025, 34(02): 342-348 (in Chinese).